Journal of Molecular Liquids 366 (2022) 120276

Contents lists available at ScienceDirect

Journal of Molecular Liquids

journal homepage: www.elsevier.com/locate/molliq

Solubility, aggregation and stability of Amphotericin B drug in pure organic solvents: Thermodynamic analysis and solid form characterization

R. Soto [a,b,*,1], P. Patel [a,1], Ahmad B. Albadarin [c], M.O. Diniz [a], S.P. Hudson [a]

[a] SSPC, Science Foundation Ireland Research Centre for Pharmaceuticals, Bernal Institute, Department of Chemical Sciences, University of Limerick, Limerick V94T9PX, Ireland
[b] Department of Chemical Engineering and Analytical Chemistry, University of Barcelona, Marti i Franquès, 1-11, 08021 Barcelona, Spain
[c] B&WB Department of Chemical Engineering and Advanced Energy, Maroun Semaan Faculty of Engineering & Architecture, American University of Beirut, Lebanon

ARTICLE INFO

Article history:
Received 28 March 2022
Revised 7 June 2022
Accepted 31 August 2022
Available online 13 September 2022

Keywords:
Amphotericin B
Thermodynamic solubility
Stability
Solid-state characterization
Aggregation

ABSTRACT

The solubility of amphotericin B (AmB) has been studied between temperatures of 298–343 K in a range of pure organic solvents including methanol, ethanol, isopropanol, butanol, acetone, tetrahydrofuran, and 1,4-dioxane. The initial solid form used in solubility determinations has been characterized by a series of techniques including powder X-ray diffraction (PXRD), scanning electron microscopy (SEM), Fourier transform infrared (FTIR) and Raman spectroscopy, thermogravimetric analysis and differential scanning calorimetry. Pure AmB melts at 444.5 K with an associated enthalpy of fusion of 177.2 kJ/mol. The equilibrated solids in suspension have been characterized by SEM and PXRD and additionally, the equilibrated saturated solutions have been characterized by in-situ UV–vis to probe the saturation and the aggregation state of AmB. In the explored solvents, in terms of mass ratio, the solubility has been found to be remarkably low, decreasing in the order: ethanol > tetrahydrofuran > butanol ≃ 1,4-dioxane ≃ isopropanol > acetone. The relative order of solubility obtained in the alcohols correlates well with their polarity, revealing important interactions of the solvents' hydroxyl group with the polyol chain and the micosamine sugar carboxylic moiety of amphotericin B. Except in dioxane and isopropanol, the obtained Van't Hoff enthalpies of solution reveal an inverse proportionality to the experimental molar fraction solubility values obtained experimentally, indicating a larger energy requirement to solvate AmB molecules. Aggregation of AmB in the equilibrated solutions was not detected in any of the solvents studied yet HPLC analyses revealed that the API degraded in methanol during the equilibration time for the solubility determinations.

1. Introduction

The solubility of an active pharmaceutical ingredient (API) is a fundamental property that must be known prior to any crystallization study since the supersaturated state refers to the solid–liquid equilibrium composition. The solubility of an API has a direct influence on its rate of reaction, crystallization, and purification and therefore it has a direct impact on the development of different drug formulations [1]. It is also paramount for drug uptake rate *in vivo* since in order to exhibit acceptable bioavailability, the drug must be soluble in the gastrointestinal tract if administered orally or must dissolve *in vivo* to be delivered by intravenous injection methods [2]. In addition, solubility data of an API is important to select preformulation strategies for toxicological, pharmacokinetic, and pharmacodynamic studies [3]. The solubility of a compound usually increases with temperature and strongly depends on the solvent studied. It is generally accepted that stronger solute–solvent interactions lead to higher solvation energies and in turn to higher solubility. However, drugs can be complex molecules containing manifold different functional groups, which makes it difficult to quantify such interactions for drug molecules and, hence the rationalization and accurate prediction of their solubility is hampered [4].

The solubility of a solid in a liquid solvent can be determined experimentally by a variety of methods [5,6]. Using analytical methods, the various phases in equilibrium are characterized by chemical analysis, while in synthetic methods a characteristic property, e.g. electrical conductivity, refractive index, etc., of the

* Corresponding author at: SSPC, Science Foundation Ireland Research Centre for Pharmaceuticals, Bernal Institute, Department of Chemical Sciences, University of Limerick, Limerick V94T9PX, Ireland.
E-mail address: r.soto@ub.edu (R. Soto).
[1] Both authors contributed equally.

https://doi.org/10.1016/j.molliq.2022.120276
0167-7322/

system is measured [5]. Among the former, static methods rely on the solubility determination when the equilibrium state is reached whereas in dynamic methods a variable of the system is modified continuously, and the variation of other parameter is followed as a function of such variable. In addition, the accurate determination of the fusion properties of the solid form along with a sound characterization of the crystalline structure and the study of the solid–liquid equilibrium thermodynamics is also crucial to improve the drugs final formulation. For example, the determination of enthalpy of fusion and melting point of the solid form of a given API has been shown to be essential towards the improvement of the prediction capability of the current models used to predict the aqueous solubility [7].

APIs can be produced via synthetic or semi-synthetic routes, involving various synthesis steps for the pursued molecules in the laboratory. APIs can also be derived from natural sources such as plants, bacteria or animal cells by suitable extraction and isolation methods [8]. Both the routes entail varieties of solvents in a considerable amount starting from solubilization of raw materials, extraction, isolation and purification/recrystallization to obtain the product of desired quality [9].

Since complete removal of a solvent is often impossible, the determination of residual solvent content in the final formulation has therefore been subjected to severe control and residual solvent limits, established by the International Council for Harmonisation (ICH). Accordingly, solvents are divided into three main groups: i) Class I solvents are carcinogenic and/or present environmental hazards and hence, they are recommended to be avoided when possible, ii) Class II solvents can cause irreversible toxicity and their use should be limited, and iii) Class III solvents are those presenting low potential toxicity to human and/or the environment and their usage has been promoted in the API manufacturing processes [10]. These are not the only attributes to be considered when choosing a solvent since other important features such as boiling point, melting point, polarity or presence of particular functional groups also play a fundamental role in the process development [11]. In terms of polarity, solvents are classically divided into polar protic (ability to accept and donate protons), polar aprotic (ability to accept protons) and non-polar (unable to accept or donate protons). As a result, the interaction between the API and the chosen solvent can vary in strength, e.g., hydrogen bonds, ionic bonds, Van der Waals interactions, and hydrophobic bonds, which impact directly on their solvation capability and thus the solubility.

Amphotericin B (AmB, $C_{47}H_{73}NO_{17}$, MW: 924.09 g/mol, see Fig. 1) is a polyene macrolide semi-synthetic antibiotic and was introduced to the market in 1959. Since then, it has been the gold standard therapeutic against systemic fungal infections and second line treatment for leishmaniasis [12,13]. AmB is isolated from *Streptomyces nodosus* via solvent extraction followed by evaporation of solvent to obtain a crude powder, which is further washed to remove the unwanted compounds and finally vacuum dried to obtain a solid with desired qualities [13]. Now amphotericin B could have a new, important medical use since when it is administered to cultured epithelial cells extracted from the lung airway linings of cystic fibrosis patients, the drug has been shown to be able to create new ion channels that replace those blocked by mutations of the cystic fibrosis transmembrane conductance regulator (CFTR) protein [14].

AmB has a high molecular weight and a complex chemical structure [15] with remarkable flexibility to rotate bonds. As highlighted in Fig. 1, it presents amphipathic and amphoteric properties due to the presence of hydrophobic polyene and hydrophilic polyol regions, attached to both a carboxylic acid group (pKa 5.7) and a basic mycosamine sugar (pKa 10) [15]. Given the increasing interest of the pharmaceutical industry on crystallizing high molecular weight compounds with structural flexibility with multiple functional groups [16], AmB becomes an excellent molecule for solubility studies in different organic solvents, in addition to being a molecule with interesting therapeutic applications in itself.

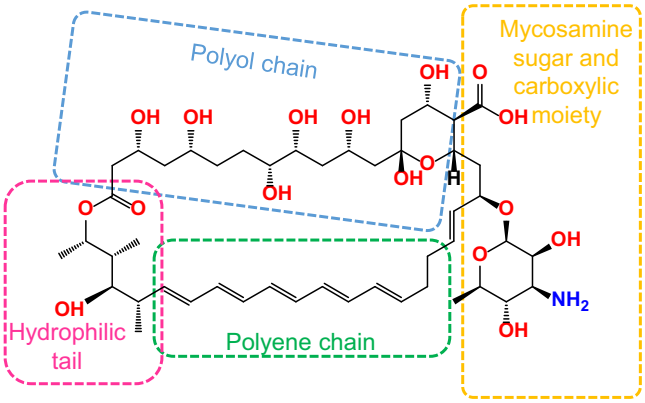

Fig. 1. Chemical structure of AmB and main groups of the macrolide molecule.

AmB belongs to BCS class IV exhibiting low solubility and poor membrane penetration, potentially due to the presence of hydrophobic polyene and hydrophilic polyols. Owing to these amphipathic properties, AmB has an ability to self-associate in an aqueous environment forming soluble monomers, dimers, oligomers and then highly toxic polyaggregates [13]. Due to its poor water solubility and membrane permeability, AmB is administered intravenously as a salt (amphotericin B deoxycholate), and in a lipid formulation (liposomal amphotericin B).

The widespread utilization of AmB is limited on account of its substantial toxicity and poor solubility in an aqueous medium. In the past, significant number of attempts have been devoted to overcome these challenges by modifying the AmB molecules through incorporation of several polar functional groups [17], solubilizing in detergent [18] or complexing agent [19]. However, no breakthrough was achieved. Due to poor water solubility in water, AmB has been adsorbed on a carrier or complexes made with surfactants to convert it into pharmaceutical dosage forms [20]. In terms of crystallization, AmB is a very difficult molecule to crystallize due to its flexible conformational structure and the absence of benzene rings. Only some modifications of AmB such as the iodoacetylamphotericin B have been successfully crystallized [17]. Interestingly, minimal information about AmB's solubility is available in the literature. Lim et al. [21] evaluated AmB solubility in dimethyl sulfoxide (DMSO), N,*N*-dimethylacetamide (DMA), N, *N*-dimethylformamide (DMF), and an equivolume mixture of methanol and chloroform at 65 °C. Rajagopalan et al. [22] reported the solubility of AmB in binary mixtures of different polyols and with ethanol. To the best of our knowledge, the solubility of AmB in various organic solvents at different temperatures is not available yet in the literature despite the crucial information that it could constitute for the development of new formulations and purification processes.

This work aims to determine the solubility of amphotericin B between 298 and 343 K in seven pure organic solvents of different chemical nature: methanol, ethanol, isopropanol, butanol, acetone, tetrahydrofuran (THF), and 1,4-dioxane. The first four solvents are polar protic, the following two are polar aprotic, and the last one is a non-polar solvent. Thermodynamic modelling of solubility data will allow the development of accurate predictive models. This along with a sound characterization of the solid phase of this complex molecule are important for the future rational development of AmB therapeutics.

2. Experimental

2.1. Chemicals

Amphotericin B (CAS: 1397-89-3) was acquired from Sigma Aldrich Ireland with a minimum purity of 98 %. Regarding the solvents, methanol (MeOH; CAS: 67-56-1, ≥ 99.9 %GC), ethanol (EtOH; CAS: 64-17-5, ≥ 99.9 %GC), isopropanol (IPrOH; CAS: 67-63-0, ≥ 99.9 %GC), *n*-butanol (BuOH; CAS: 71-36-3, ≥ 99.9 %GC), tetrahydrofuran (THF; 109-99-9, ≥ 99.9 %GC) and acetone (ACTN; 67-64-1, ≥ 99.9 %GC) were all purchased from Fisher Scientific ltd. (Ireland) and 1-4 dioxane (CAS: 123-91-1, ≥ 99.9 %GC) was supplied by Sigma Aldrich. All chemicals were used without further purification. Table 1 summarizes some important physicochemical properties of the solute and solvents used. The dimensionless normalized solvatochromic solvent polarity parameter (E_T^N, Table 1) accounts for the solvent polarity [23] and ranges from 0.000 (tetramethylsilane) to 1.000 (water). It represents a quantification of the solvatochromic solvent polarity parameter $E_T(30)$ defined by Dimroth and Reichardt [23,24], which indeed refers to the molar transition energy (E_T) for the longest-wavelength solvatochromic absorption band of the pyridinium *N*-phenolate betaine dye.

2.2. Experimental setup and procedure for solubility determinations

The solubility of AmB in the mentioned set of organic solvents was determined using the gravimetric method [28] within the range of temperature 298–343 K. For methanol, acetone and THF the studied range of temperature was reduced given the volatility of these solvents (please refer to boiling points reported in Table 1). The procedure consisted of preparing suspensions (visible excess solid) of AmB in the studied solvents to be equilibrated at the studied temperatures. The solutions were prepared in 30 mL vials with PTFE-coated magnetic bars that were immersed in a thermostatic bath and stirred at 1000 rpm (2mag submergible stirring plate) for at least 24 h to ensure solid–liquid equilibrium. Before sampling, the stirrer was switched off for two hours to let the solids in the suspension settle. Since the solubility was expected to be low, notably large aliquots of approximately 10-15 mL of the equilibrated solutions were taken to maximize the amount of solute remaining after solvent evaporation enabling it to be weighed on a five decimal precision balance (Mettler Toledo. Model No: XP205). These aliquots were transferred to evaporation vials after filtration using 200 nm PTFE filters. The evaporation vials were weighed empty (including the lid), after transferring the filtered equilibrated solutions, and finally weighed again after solvent evaporation. Finally, the mass ratio solubility of AmB as $g_{solute}/g_{solvent}$ was calculated at each temperature and in each solvent using Eq. (1).

$$c^*(g_{solute}/g_{solvent}) = \frac{m_{\text{vial + cap + solid}} - m_{\text{vial + cap}}}{m_{\text{vial + cap + solution}} - m_{\text{vial + cap + solid}}} \quad (1)$$

The mole fraction solubility was later computed calculated from the mass ratio solubility (C^*) using Eq.2.

$$x_{eq} = \frac{c^* \cdot M_2}{(c^* \cdot M_2 + M_1)} \quad (2)$$

being M_1 and M_2 stand for the molecular weights (g/mol) of solute and solvent, respectively.

Moreover, the UV–vis spectra of the equilibrated solutions in different solvents were recorded *in-situ* at some temperatures while aiming to assess the aggregation state of AmB. Finally, samples from the slurry in all solvents were also collected at the maximum temperature (at which any possible solution-mediated polymorphic transformation would be more noticeable) and analysed by PXRD after filtration of the solids in suspension to confirm the polymorphic form of AmB in the equilibrated suspensions.

2.3. Study of aggregation state by characterization of equilibrated solutions

The aggregation states of solubilised AmB in organic solvents at different temperature were assessed using an in-situ UV–vis probe (MCS 651 UVC CLD600, Carl Zeiss). The *in-situ* UV probe was dipped into vials of different AmB solutions kept in a water bath to maintain the temperature in order to obtain real time–temperature absorption spectra from 200 to 600 nm. Prior to taking a spectrum of an AmB solution, baseline spectra of blank solvents at different temperatures were recorded. A solution of AmB obtained after filtration was diluted suitably and the absorption spectra were recorded ranging from 200 to 600 nm.

2.4. Solid state characterization of initial AmB, equilibrated solute and of equilibrated solids in suspension

The as received amphotericin B solid and occasionally the solids in suspension in equilibrated solutions were characterized by the following set of techniques. Powder X-ray diffraction patterns were collected in an Empyrean PANalytical diffractometer using a Cu radiation source (λ = 1.541 nm) at 40 mA and 40 kV. Scans were performed in the 2 Θ angle range 5 – 35° using a step size of 0.01° (99.5 s duration at each step and scan speed of 0.034°/s). SEM micrographs were taken in a Hitachi SU-70 instrument operated at 5 kV being the samples carefully mounted onto carbon tape and coated with gold. Solid state FTIR spectra were collected in a Perkin Elmer Spectrum 100 instrument equipped with an attenuated total reflectance (ATR) accessory in the wavenumber range 650–4000 cm^{-1} with a resolution of 4 cm^{-1} and 16 accumulations. The sample was presented to the instrument diamond/ZnSe crystal of the press zone e.g., without further modification such as crushing, and the force applied to the sample was adjusted to ensure well-defined quality absorption bands and reproducibility. Background spectra were acquired previously without sample and automatically subtracted to the sample spectra. Solid state Raman was performed using a Kaiser Raman RXN2 device with 400 mV laser power and wavelength of 785 nm using a resolution of 1 cm^{-1}, an accumulation of 5 scans and an exposure time of 1 s within the Raman shift range 100–3425 cm^{-1}.

Thermogravimetric analysis (TGA, Perkin Elmer TGA 4000) and differential scanning calorimetry (DSC, Perkin Elmer Pyris I) were performed to assess the thermal behaviour of the as received AmB. For TGA 5–10 mg of sample were used with a heating program consisting of a single ramp 10 °C/min at from 30 to 950 °C under N_2 flow of 20 mL/min. For DSC, the furnace cell was pre-calibrated against the melting properties of indium metal. 2–6 mg of solid were placed in hermetic Tzero closed aluminium pans and the heating program was set from 30 to 250 °C using a heating rate of 10 °C/min under inert N_2 flow of 20 mL/min. In addition, Karl-Fisher titration (Hanna Instruments HI903, Karl Fisher titrator) was performed on the raw AmB material using a standard operating procedure.

A reverse phase high performance liquid chromatography (RP-HPLC) method was developed in house to assess the stability of AmB equilibrated solids in suspension and of the solute in the equilibrated saturated solutions in the respective organic solvents at the highest temperature studied. For the equilibrated solids in suspension, these were isolated by vacuum filtration, dried and then redissolved in a DMSO:MeOH (1:9 vol%) mixture before injecting immediately to the HPLC. For the solute in the equilibrated saturated solutions, these were recovered after solvent

Table 1
Summary of relevant physical properties of Amphotericin B and the solvents studied.

Substance	MW [g/mol]	T_m [K]	T_b [K]	ρ[a] [g/cm^3]	μ[a] [cP]	δ[b] [J/cm$^{3/2}$]	E_T^N [c] [–]	Class[d]
MeOH	32.04	175.6	337.8	0.792	0.545	29.3	0.762	2
EtOH	46.07	159.0	351.4	0.788	0.963	26.0	0.654	3
IPrOH	60.09	184.0	355.8	0.786	1.904	23.7	0.546	3
BuOH	74.12	183.3	390.8	0.810	2.613	23.3	0.586	3
Diox	88.11	284.9	374.2	1.033	1.172	19.7	0.164	2
THF	72.11	165.2	339.2	0.888	0.480	19.0	0.207	2
ACTN	58.08	178.5	329.2	0.785	0.295	22.1	0.355	3
AmB	924.1	447.2[e]	–	–	–	25.1[f]	–	–

[a] Density and viscosity at 298 K and 1 atm from the software Aspen Hysys v.10.0 database. [b]Hildebrand solubility parameter (δ) of solvents [25]. [c]Dimensionless normalized solvatochromic solvent polarity parameter [23]. [d]Classification according to the ICH Harmonised guide. [e] From [26]. [f] Estimated from the group contribution method based on first-order UNIFAC groups described in Hansen (2007) [27].

evaporation and redissolved using the same procedure described. The HPLC consisted of an Agilent 1200 Infinity Series (Agilent Technologies, Palo Alto, USA) equipped with a G1311B 1260 quaternary pump, G1329B 1260 ALS autosampler, G1316A 1260 TCC (thermostated column compartment), G1365D 1260 MWUV detector and an Agilent InfinityLab Poroshell 120 EC-C18 (4.6 × 100 mm, 2.7 μm) column. The acquired data were processed using OpenLAB CDS Chemstation software. The mobile phase consisted of a mixture of acetonitrile: disodium EDTA (0.005 M) buffer (30:70 v/v) at a flow rate of 1 mL/min that led to a retention time of 11.25–12.50 min when detection was carried out at 405 and 381 nm. The assay was linear (R^2 = 0.9994) in the concentration range 1–200 μg/ml.

2.5. Evaluation

Several empirical or semiempirical thermodynamic models (Eqs. 3–5) have been applied to obtain solubility expressions that enable the interpolation of accurate solubility values within the range of temperature explored. Eq. (3) is a widely used fully empirical relationship, Eq. (4) is the Buchowski– Książczak semi empirical equation [29], and Eq. (5) is derived from the Clausius-Clapeyron equation and referred to as the Apelblat semi empirical relation [30,31].

$$\ln x_{eq} = \frac{c_1}{T^2} + \frac{c_2}{T} + c_3 \tag{3}$$

$$\ln\left[1 + \frac{\lambda(1 - x_{eq})}{x_{eq}}\right] = \lambda h\left[\frac{1}{T} - \frac{1}{T_m}\right] \tag{4}$$

$$\ln x_{eq} = A + \frac{B}{T} + C\ln(T) \tag{5}$$

The parameters involved in Eqs. 3–5 (c_1, c_2, c_3, λ, h, A, B and C) were estimated by non-linear regression through Matlab scripts using the function lsqnonlin that minimizes the differences between experimental and calculated solubility values as objective function, i.e. the total sum of squared residuals (*TSSR*), which equals $\Sigma(x_{exp}\text{-}x_{cal})^2$.

In addition, the experimental molar fraction solubility values determined were used to estimate the Van't Hoff enthalpy change ($\Delta^{vH}_{sln}H°$) by linearization of Eq. (6). Please note that these are not the true calorimetric values of the enthalpy of solution, which would include information about the activities of the involved species but, simply refer to the temperature dependence of solubility [32].

$$\left(\frac{\partial \ln x_{eq}}{\partial \ln(1/T)}\right) = -\frac{\Delta^{vH}_{sln}H^{\circ}}{R} \tag{6}$$

3. Results and discussion

3.1. Solid form characterization

Fig. 2 presents the X-ray diffractograms of the solids in suspension collected from the slurry of the equilibrated solutions in the solubility experiments, showing some defined diffraction bands that confirm a certain degree of crystallinity. The as received AmB material showed a characteristic diffractograms of a crystalline material with preferential orientation in the diffraction bands located at 2Θ angles of 4.90°, 14.05° and 21.80°. Noteworthy, no reference was found in the Cambridge Crystallographic Data Centre (CCDC) for a crystalline form of AmB and therefore identification of the solid form according to the CSD was not possible. The diffractograms of the equilibrated solids in suspension collected in the different solvents studied at the highest temperature explored in the solubility determinations presented the same characteristic peaks in the same location as the starting material, indicating that no transformation of the solid form occurred during the equilibration. The diffractograms collected are in coherence in terms of the most significant diffraction bands and intensity with those reported by Y. Zu et al. [33], by Chomchalao et al. [34] and by Yen et al. [35] for solid AmB.

Fig. 3 shows representative examples of the as received AmB showing a spherulitic structure formed by an agglomeration of elongated particles. This particular shape has already been reported for other APIs such as curcumin [36]. These structures typically originated from crystallization at very high supersaturations resulting in spherulitic or dendritic morphologies as a result of adhesive growth [37]. The fact that the spherulites broke during the sample preparation despite extreme care being taken to manipulate them suggest that these structures are very brittle in nature. Interestingly, SEM images of crystalline pure AmB are not abundant in the literature and comparison of this peculiar morphology has only been possible with the micrographs reported by Zu et al. [33] which exhibited an irregular dendritic morphology, in agreement with our observations. Accordingly, it is difficult to infer whether such peculiar morphology arises from the method of isolation of the raw material. With regards to the solids in suspension from the equilibrated solutions, further SEM images can be found in the *Supporting Information* (Figure S1). The morphology was quite similar to that of the original solid used indicating that in principle the particles remained unchanged during the solubility experiments.

Fig. 4 shows the TGA and DSC patterns obtained for the as received AmB. Regarding the thermal analysis by TGA and SDTA, our results showed a constant weight loss that stabilized at about 500 °C (773.15 K). These results are in agreement with those reported by Mehenni et al. [19] for pure AmB. The initial weight loss of about 5–7 % up to 105 °C can be related to a dehydration

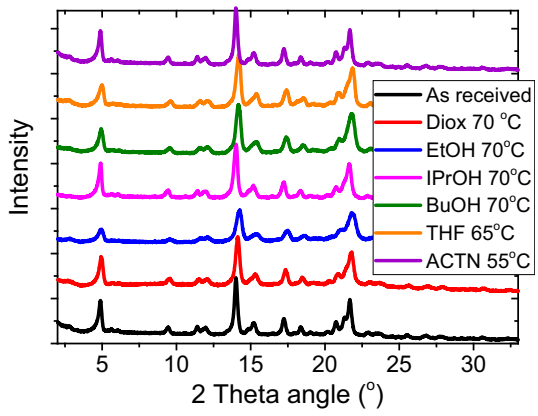

Fig. 2. PXRD diffractograms collected for the solid AmB as received and the solids in suspension for the equilibrated solutions in the studied solvents at the maximum corresponding temperature.

step through which moisture trapped within the AmB structure are released. This is consistent with the water content of 6.72 %wt determined by Karl-Fisher titration of the as received AmB. Afterwards, the mass loss is stabilized up to 150 °C, being followed by a loss of about 10 % of initial mass that can be related to the beginning of the decomposition of AmB, which further decomposed up to 500 °C.

With respect to DSC analyses, the thermogram showed a clear sharp endothermic peak at 171.3 °C (444.5 K), which is very similar to the thermogram reported by Mehenni et al. [19] for pure AmB, suggesting a crystalline material with a melting point of 174 °C (447.15 K). These authors also reported a glass transition temperature at 200 °C, which is somewhat in agreement with our results since this behaviour could be inferred as well from the baseline vertical drift observed after the melting in Fig. 4b. Melo et al. [38] reported a melting temperature onset value of 164.9 °C (438.05 K), which is in agreement with our results yet their thermogram was notably less clear in terms of the sharpness of the reported thermal events and also showing some sort of baseline instability. Unfortunately, the melting enthalpy of 177.17 kJ/mol obtained in this work cannot be compared with previous studies since, to the best of our knowledge, there are no fusion enthalpy ($\Delta^{\circ}H_f$) values for solid AmB reported in the literature. This is probably due to the beginning of the decomposition of AmB molecule above 150–160 °C as evidenced from TGA analysis and the possible mentioned glass transition occurring simultaneously close to the melting point. Even though, our value might not be sufficiently accurate because of these difficulties, our melting enthalpy is comparable to those reported for 2,5-di-*n*-nonadecyloxy-1,4-benzoquinone (150.2 kJ/mol), and for significantly large molecules including long paraffin chains such as glyceryl tripalmitate (179.4 kJ/mol), glyceryl tristearate (203.3 kJ/mol), glyceryl trimyristate (152.4 kJ/mol), hexacontane (186.8 kJ/mol) and *n*-pentacontane (185.0 kJ/mol) [39].

Fig. 5 depicts the collected FTIR and Raman spectra for the solid AmB as received. In the infrared spectrum, the asymmetric and symmetric characteristic vibrations of the —OH group as broad bands are observed at 3000–3350 cm^{-1} (please refer to the *Supporting Information* for the full IR spectra). As these bands are weak, no significant intra or intermolecular (aggregation) of the AmB molecules are indicated [40]. The main absorption bands according to the literature [40], are present, i.e. the —OH bending out of plane (668 cm^{-1}), the pyranose ring breathing (764.6 and 795 cm^{-1}), the peaks due to —CH_3, COO^- and —NH_2 bending out of plane (840 cm^{-1}), the bending in plane associated with the chromophore and the —CH in transpolyene out of plane bending (1006 and 1039 cm^{-1}), the bending out of plane attributable to NH_2 (1067 cm^{-1}) and the C—O—C pyranose ring. The band at 1008 cm^{-1} can be associated with the —CH polyene groups [38]. In addition, the vibrations at about 1067, 1132 and 1163 cm^{-1} have been ascribed to the C—O asymmetric stretch (COC, COH) [40]. The COC=O asymmetric stretch of the β glycosidic linkage is related to the absorption band at 1186 cm^{-1}, the —CH in plane bend polyene is observed at 1401 cm^{-1}, which is the polyene C=C stretch observed at 1555 cm^{-1}, and finally the symmetric stretching for COO^- arises as a clear band at 1690 cm^{-1}. The Raman spectrum of the as received material showed three well defined absorption bands at 1002, 1155 and 1555 cm^{-1}, which are in excellent agreement with the literature [19], and are related to the C—C—H, C—O and C—C bonds respectively.

Stability of the AmB solids in suspension at the highest equilibrated temperature was determined by HPLC, see Fig. 6. Though the degradation studies of AmB in various aqueous and non-aqueous solvents and mixture of thereof has been determined previously [21,41], it is still not available in pure organic solvents. Of the solvents used in this study, methanol was the only solvent that showed degradation of AmB while no signs of degradation were observed in the rest of the solvents (Fig. 6). The small peaks that arise just before the main AmB peak could be attributed to the presence of impurities coming from the AmB synthesis since they are observed in the as received AmB as well. Please note that the retention time drift to the left in Fig. 6 butanol series is due to interday systemic analytical variation. Despite showing apparently higher solubility in methanol (data not shown), it was omitted from this work because of the observed degradation. Furthermore, to confirm the degradation of AmB in the presence of methanol only, the solute from different saturated solutions at equilibrium, collected after solvent evaporation, were also analysed by HPLC.

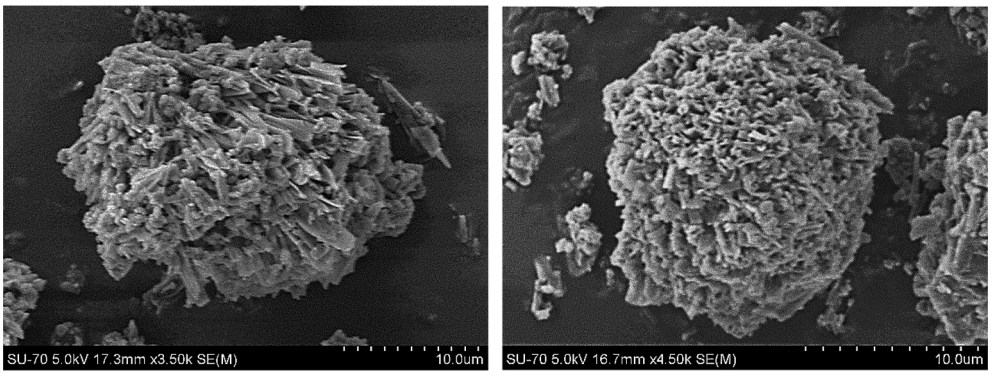

Fig. 3. SEM images of the as received AmB used in the solubility experiments. Scale bars refer to 10 μm.

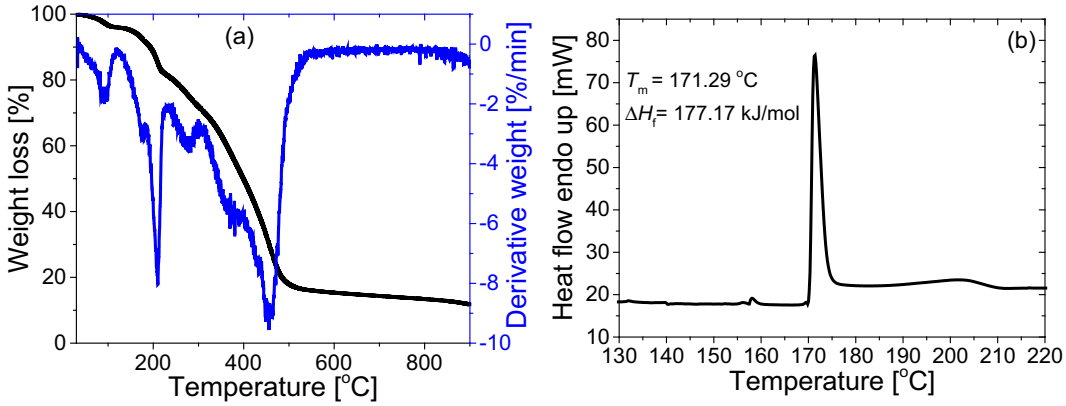

Fig. 4. TGA and SDTA curves (a) and DSC thermogram of as received AmB (b).

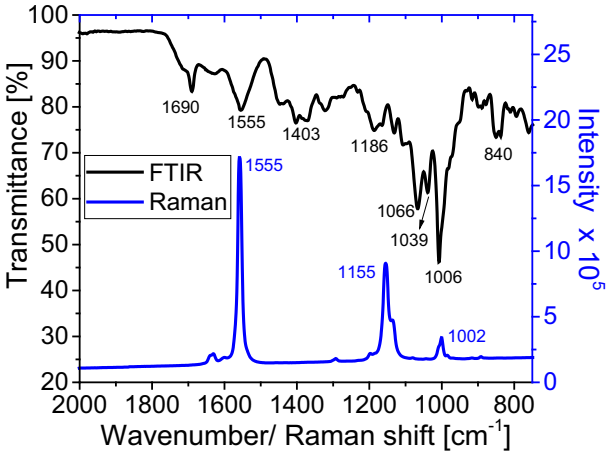

Fig. 5. Solid state FTIR and Raman spectra of as received AmB.

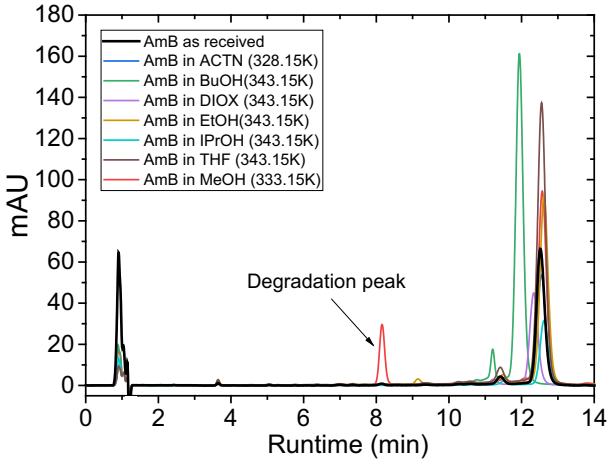

Fig. 6. HPLC chromatogram of AmB equilibrated solids in suspension in the studied solvents at the maximum temperature explored for each case.

It was confirmed thereby that AmB showed degradation only in methanol (Figures S2 and S3).

3.2. Solubility and thermodynamic analysis

Table 2 gathers the solubility data obtained in terms of mass ratio for AmB in the studied solvents at different temperatures. In general, the solubility decreased in the order: EtOH > THF > BuOH ≃ Diox ≃ IPrOH > ACTN. For alcohols, the relative order of solubility obtained correlates well with the normalized solvatochromic solvent polarity parameter (E_T^N, Table 1), which suggest significant interactions of the hydroxyl group of alcohols with the polyol chain and the micosamine sugar carboxylic moiety of AmB. This explanation is further supported by the positive charges observed in the charge density representation of the AmB molecule in an optimized geometry depicted in Fig. 7. However, for the rest of solvents the rank of solubility obtained is not properly described by the E_T^N parameter, since for instance, the solubility in THF (moderately polar) is significantly higher than that obtained in ACTN, which suggest that solvation of AmB molecule is an intricate phenomenon given the complexity of the solute molecule having several moeties with different functionalities. Unfortunately, comparison with the literature was not possible for most of the solvents studied due to the lack of reported solubility data of AmB in organic solvents. Only for ethanol, Rajagopalan et al. [22] reported a value of < 0.06 mg/mL, which is lower than our value, corresponding approximately to 0.16 mg/mL at 298 K. Noteworthy, the above discussion explaining the rank of solubility observed experimentally for AmB could be extrapolated to its congener Amphotericin A (AmA) since the main structural difference between both molecules is that one of the seven conjugated double bonds in AmB is saturated in the AmA, being therefore the most prone polar moieties toward interaction, the micosamine sugar and the polyol chain, identical in both antibiotics.

Further evaluation of the Hildebrand solubility parameters (δ, Table 1) reveals that, except for alcohols, there is no clear correlation with the experimental solubility values determined. The δ solubility parameter provides a numerical estimate of the solute–solvent interactions and it is generally accepted that the closer its value is between solute and solvent, the higher is the solubility expected in this solvent. Nonetheless, it often underestimates the solubility in those systems of polar nature where hydrogen-bonding plays a significant role [27] and for which more complicated three-dimensional solubility parameters, e.g., Hansen solubility parameters, are more appropriate.

Table 3 summarizes the estimated parameters obtained by non-linear regression of Eqs.3–5 using the experimental molar fraction solubility data. Generally, Eq. (3) and Eq. (5) provided the best fitting, which can be ascribed to the higher number of parameters in both empirical equations in comparison with the Buchowski–Książczak semi empirical equation (Eq. (2)). Fig. 8 depicts the experimental molar fraction solubility values used in the modelling along with the fitting of Eq. (3), which is excellent in most of the cases. Interestingly, the relative solubility order in terms of

Table 2
Mass ratio solubility of AmB in the studied solvents in the range of temperature 298.15–343.15 K and associated standard deviations (SD) for the triplicate measurements. Only significant figures are given.

	$g_{solute}/g_{solvent}$ ± SD					
T [K]	EtOH	IPrOH	BuOH	Diox	THF	ACTN
343.15	0.00090 ± 0.00006	0.00047 ± 0.00009	0.00046 ± 0.00002	0.00037 ± 0.00002	–	–
338.15	0.00077 ± 0.00007	0.00037 ± 0.00007	0.00038 ± 0.00007	0.00035 ± 0.00003	0.00061 ± 0.00098	–
333.15	0.0007 ± 0.0001	0.00030 ± 0.00002	0.00030 ± 0.00009	0.00031 ± 0.00004	0.00048 ± 0.00009	–
328.15	0.00059 ± 0.00004	0.00022 ± 0.00005	0.00026 ± 0.00004	0.00027 ± 0.00003	0.00040 ± 0.00002	0.00029 ± 0.00009
323.15	0.00047 ± 0.00004	0.00018 ± 0.00001	0.00022 ± 0.00001	0.00024 ± 0.00002	0.00033 ± 0.00004	0.00021 ± 0.00001
318.15	0.00046 ± 0.00002	0.00016 ± 0.00002	0.00021 ± 0.00001	0.00020 ± 0.00003	0.00025 ± 0.00009	0.00015 ± 0.00003
313.15	0.00035 ± 0.00002	0.00013 ± 0.00002	0.00013 ± 0.00004	0.00016 ± 0.00003	0.00017 ± 0.00003	0.00010 ± 0.00001
308.15	0.00025 ± 0.00001	0.00010 ± 0.00002	0.00010 ± 0.00001	0.00013 ± 0.00002	0.00014 ± 0.00005	0.00007 ± 0.00002
303.15	0.00022 ± 0.00003	0.00009 ± 0.00001	0.00008 ± 0.00002	0.00009 ± 0.00001	0.00013 ± 0.00002	0.00004 ± 0.000001
298.15	0.00020 ± 0.00002	0.00009 ± 0.00001	0.00005 ± 0.00001	0.00007 ± 0.00001	0.00011 ± 0.00002	0.00002 ± 0.000001

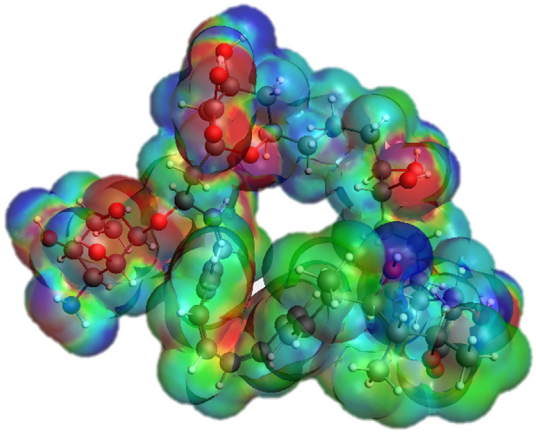

Fig. 7. Charge density representation of AmB molecule in optimized geometry created with Cosmo RS software. Red colour refers to positive charges, blue to negative charge and green to neutral charge.

molar fraction is slightly different to that reported in Table 2 as mass ratio. For molar fraction solubility values, two main groups can be distinguished: the first group being EtOH, THF and Diox, which present a comparable solubility and are almost double those measured in the second group, IPrOH, BuOH and ACTN. This suggests an important contribution of the interactions of THF and Diox with the less polar parts of AmB molecules eventually contributing to a better solvation.

For an ideal solution, the solubility can be predicted by Eq. (7), as a function of the molar enthalpy of fusion and the melting temperature.

$$\ln x_{eq}^{ideal} = -\frac{\Delta H_m}{R}\left(\frac{1}{T_m} - \frac{1}{T}\right) \quad (7)$$

Using the melting data determined by DSC and depicted in Fig. 4b, the ideal mole fraction solubility values between 298 and 343 K range from $1.2{\cdot}10^{-10}$ – $1.1{\cdot}10^{-6}$. The values are from 2 to 5 orders of magnitude lower than those determined experimentally in the studied solvents, which indicate negative activity coefficients and therefore favourable interactions between the AmB and the solvents. Even though our melting enthalpy values can be taken as an estimation due to the mentioned difficulties in analysing the DSC data, the present analysis can still be considered valid because the difference between ideal and actual solubilities are so significant that the mentioned discussion in terms of the activity would remain unaltered.

In the present investigation, an in-situ UV–vis probe was used to determine the conformation and aggregation state of AmB (solute) in saturated solutions at different temperatures, see Fig. 9. It is important to note that the solvent spectra were subtracted in all cases. In solution, AmB can exist in three states including monomers, aggregates and super-aggregates [15]. As extensively described in the literature, the toxicity and the effectiveness of AmB differs based on its aggregation state. UV spectroscopy has been demonstrated to be an effective technique to assess the aggregation state. In the studied organic solvents, AmB exists as a monomeric form, as evidenced from the UV spectra collected at different saturation temperatures (Fig. 9), which show four clear peaks with maxima at 348(I), 368(II), 382(III) and 410(IV) nm. The predominance of the monomeric state is confirmed by the presence of the peak at 410 nm, in agreement with the literature [42]. The ratio of the absorbance of peak I to peak IV (A_{348}/A_{410}) was taken into account to measure the extent of aggregation AmB. Typically, this ratio is below (<2) for the monomeric state, while it is above 2 for aggregated species [42]. These are exemplified by some of the marketed formulations, for instance, Fungizone® and AmBisome® presenting A_{348}/A_{410}values of 2.9 and 4.8, respectively [43]. The A_{348}/A_{410} ratio of all saturated solutions at different temperatures was found to be below 2, showing the high-

Table 3
Estimated parameters for the solubility equations evaluated (Eqs. (3), 4, and 5) for AmB in the studied solvents. *TSSR* refers to the total sum of squared residuals from each model.

Parameter	EtOH	IPrOH	BuOH	Diox	THF	ACTN
c_1	−2553.1	4,810,548	−2542.6	−5420286	−1276.5	−948.8
c_2	−3437.1	−34057.9	−4299.4	30061.7	−4745.5	−7454.0
c_3	0.0341	47.99	2.338	−51.83	4.086	11.815
$TSSR_{,Eq.3}{\cdot}10^{10}$	0.143	0.015	0.203	0.017	0.126	0.009
λ	0.000337	0.000532	0.000304	0.000250	0.001227	0.007541
h	9509597.8	8,349,271	11,310,700	12,162,401	3,789,809	1,000,150
$TSSR_{,Eq.4}{\cdot}10^{10}$	0.159	0.088	0. 388	0.319	0.125	0.009
A	176.71	−623.11	281.90	−86.864	−122.19	−173.69
B	−11920.8	25544.5	−17756.11	833.021	1275.78	1273.48
C	−26.034	92.200	−41.176	12.720	18.625	27.427
$TSSR_{,Eq.5}{\cdot}10^{10}$	0.121	0.016	0.177	0.345	0.119	0.012

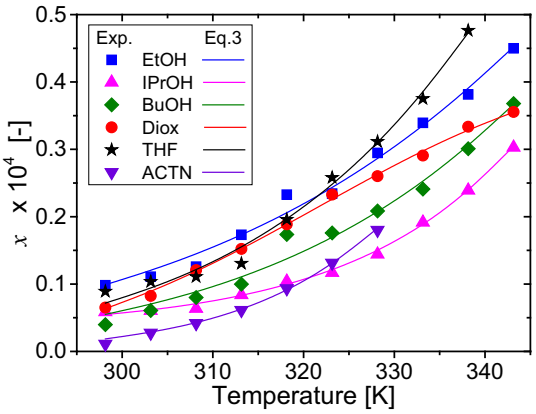

Fig. 8. Experimental molar fraction solubility (symbols) and fitting provided by Eq. (3) (solid lines).

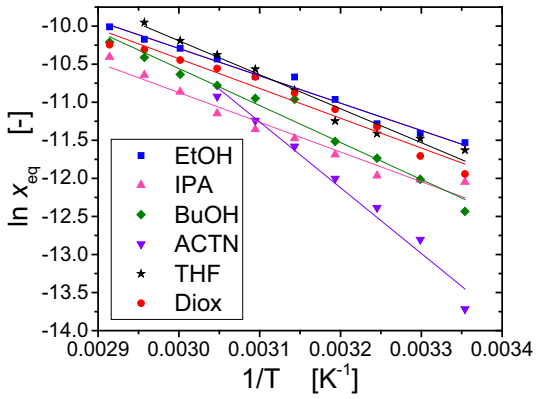

Fig. 10. Van't Hoff plot of molar fraction solubility values obtained for AmB in the solvents studied.

est value (0.92) in THF at $T_{55°C}$, whereas the lowest ratio (0.0066) was exhibited in IPrOH at $T_{55°C}$. Overall, the reported UV–vis absorbance increased with the saturation temperature in all the cases, indicating a larger amount of AmB dissolved in a monomeric form. Moreover, the relative level of absorbance at the same temperature among the solvents studied was in agreement with the relative order of solubility results reported in Table 2.

The Van't Hoff enthalpies of solution of AmB in the studied solvents were obtained from the experimental molar fraction solubility values by linearization of Eq. (6), as depicted in Fig. 10. As expected, all the estimated enthalpy values revealed an endothermic scenario for the dissolution of AmB in the studied solvents. The estimated values, the associated uncertainty and the determination coefficient are detailed in Table 4. In general, good linear trends were obtained with R^2 values higher than 0.96. However, it was observed that such linearity was not always maintained at the minimum temperatures, e.g. the case of acetone in Fig. 10. It is to be noted that indeed the Van't Hoff plot does not necessarily render a linear trend and that in some cases nonlinear profiles are obtained by definition, as demonstrated for the solubility of several APIs in organic solvents [44]. $\Delta^{vH}_{sln}H°$ merely reflects the temperature dependence of solubility since it neglects the effects of the activity coefficient [45,46]. The assessment of the $\Delta^{vH}_{sln}H°$ values reveals a correlation, although not perfectly clear in all cases (IPrOH), by which the higher the solubility the lower the values of $\Delta^{vH}_{sln}H°$. This indicates that more energy is required to dissolve a mole unit of AmB in those solvents in which a higher enthalpy of solution was obtained. Nordström and Rasmuson [46] previously linked this experimental fact to a steeper slope (dependence of solubility upon temperature) since all the solubility curves tend to the same point of convergence at the solid melting point. Perhaps, our $\Delta^{vH}_{sln}H°$ value determined in acetone appears to be a bit high, which can be explained by the low solubility value determined at the lowest temperature explored (Fig. 10) that significantly influences an increase in the slope for the corresponding linear plot.

4. Conclusions

From the thermogravimetric solubility study performed for AmB in several organic solvents, in terms of mass ratio the solubil-

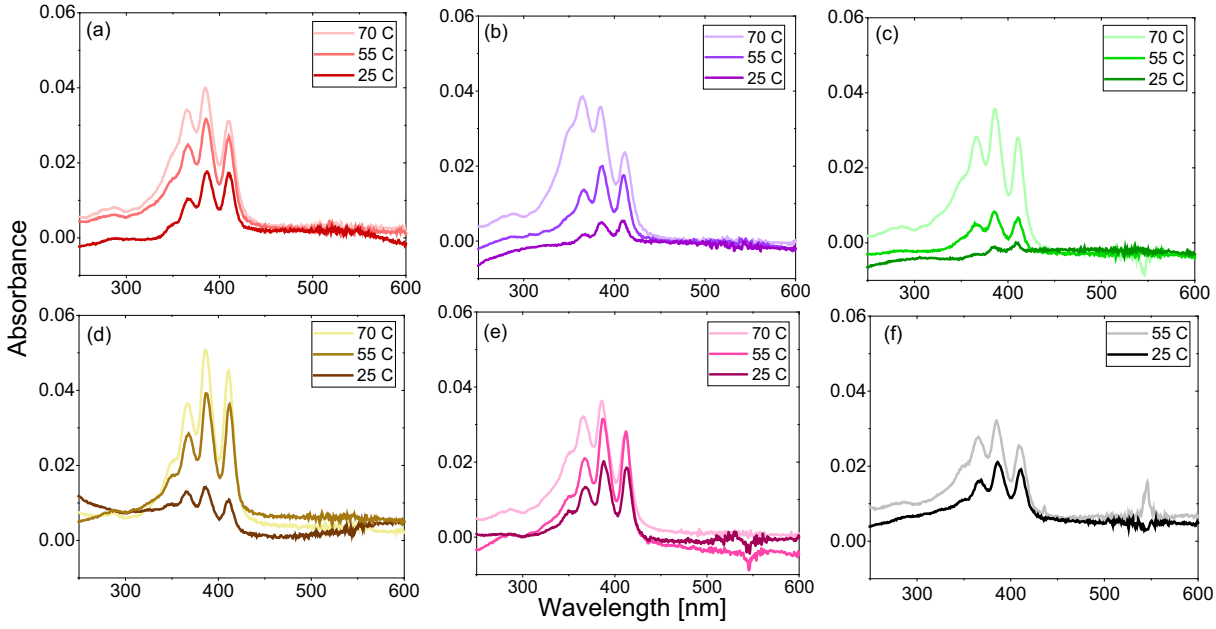

Fig. 9. UV–vis spectra collected for the saturated solutions at different temperatures in: (a) EtOH, (b) IPrOH, (c) BuOH, (d) THF, (e) DIOX, and (f) ACTN.

Table 4
Estimated Van't Hoff enthalpies of solution from molar fraction solubility data. Uncertainties are referred to the standard error.

	EtOH	IPrOH	BuOH	Diox	THF	ACTN
$\Delta^{vH}_{sln}H^o$ [kJ/mol]	29.88 ± 1.30	32.46 ± 2.20	40.41 ± 2.37	32.52 ± 2.08	37.11 ± 2.32	71.82 ± 5.08
R^2	0.99	0.96	0.97	0.97	0.97	0.98

ity of AmB decreases in the order EtOH > THF > BuOH ∼ Diox ∼ IPrOH > ACTN, whereas in terms of mole fraction, it decreases in the order EtOH ∼ THF ∼ Diox > BuOH > IPrOH ∼ ACTN. Such differences in solubility are less significant in terms of mole fraction than in mass ratio. In general, the highest solubility is obtained in the polar protic solvents, which exhibit the highest polarity. In general, the scenario studied reveals that solubility of AmB in the studied solvents is benefited from the capability of the solvents to hydrogen bond the different solute moieties that enable such interaction, e.g. interactions of the solvent's hydroxyl group with the polyol chain and the micosamine sugar carboxylic moiety. Empirical and semi-empirical thermodynamic data have been fitted to the experimental solubility values obtained and provide mathematical expressions to interpolate the solubility of this API within the temperature range explored. Pure AmB melts at 171.3 °C (444.5 K) and the solid form studied does not transform in solution under the experimental conditions explored, as confirmed by PXRD. No signs of aggregation were observed from UV–vis analysis of the equilibrated solutions. However, degradation of AmB was observed in methanol, as confirmed by additional peaks in HPLC analysis of the dissolved AmB. The obtained Van't Hoff enthalpies of solution correlate relatively well with the solubility order obtained except for dioxane and isopropanol. A thermodynamic analysis comparing the ideal solubility to the values determined herein reveals negative activity coefficients, suggesting favourable interactions between the AmB molecule and the studied solvents.

CRediT authorship contribution statement

R. Soto: Conceptualization, Methodology, Software, Validation, Formal analysis, Investigation, Resources, Data curation, Writing – original draft, Writing – review & editing, Visualization, Supervision, Project administration. **P. Patel:** Conceptualization, Methodology, Software, Validation, Formal analysis, Investigation, Resources, Data curation, Writing – original draft, Writing – review & editing, Visualization, Supervision, Project administration. **Ahmad B. Albadarin:** Supervision, Writing – original draft, Writing – review & editing, Funding acquisition. **M. Diniz:** Investigation, Data curation. **S.P. Hudson:** Supervision, Writing – original draft, Writing – review & editing, Data curation, Project administration, Funding acquisition.

Declaration of Competing Interest

The authors declare that they have no known competing financial interests or personal relationships that could have appeared to influence the work reported in this paper.

Acknowledgement

The authors are grateful for the support of Science Foundation Ireland Research Centre for Pharmaceuticals (SSPC) grant no 12/RC/2275_P2 and to Dr. Rabah Mouras for his help with the creation of the charge density diagram using COSMO-RS software.

Appendix A. Supplementary material

Supplementary data to this article can be found online at https://doi.org/10.1016/j.molliq.2022.120276.

References

[1] J. Yousefi Seyf, A. Haghtalab, Measurement and Thermodynamic Modeling of the Solubility of Lamotrigine, Deferiprone, Cefixime Trihydrate, and Cephalexin Monohydrate in Different Pure Solvents from 283.1 to 323.1 K, J. Chem. Eng. Data. 61 (2016) 2170–2178, https://doi.org/10.1021/acs.jced.6b00163.
[2] V.M. Rao, R. Sanghvi, H.J. Zhu, Solubility of pharmaceutical solids, in: Y. Qiu, Y. Chen, G.G.Z. Xhang, L. Liu, W. Porter, V. Rao (Eds.), Dev. Solid Oral Dos. Forms Pharm. Theory Pract, 2nd ed., Elsevier Science & Technology, 2017, pp. 3–22, https://doi.org/10.1016/B978-0-12-802447-8.00001-7.
[3] J.M. Aceves-Hernández, J. Hinojosa-Torres, I. Nicolás-Vázquez, R.M. Ruvalcaba, R.M.L. García, Solubility of simvastatin: A theoretical and experimental study, J. Mol. Struct. 995 (2011) 41–50, https://doi.org/10.1016/j.molstruc.2011.03.048.
[4] Y. Zhao, W. Liu, X. Pei, D. Yao, Refinement of the theoretical solubility model and prediction of solute solubility in mixed solvent systems, Fluid Phase Equilib. 437 (2017) 43–55, https://doi.org/10.1016/j.fluid.2017.01.006.
[5] G.T. Hefter, R.P.T. Tomkins, The Experimental Determination of Solubilities, 1st ed., John Wiley & Sons Ltd, Chichester, England, 2003.
[6] L. Yang, Y. Zhang, J. Cheng, C. Yang, Solubility and thermodynamics of polymorphic indomethacin in binary solvent mixtures, J. Mol. Liq. 295 (2019), https://doi.org/10.1016/j.molliq.2019.111717 111717.
[7] C.M. Wassvik, A.G. Holmén, C.A.S. Bergström, I. Zamora, P. Artursson, Contribution of solid-state properties to the aqueous solubility of drugs, Eur. J. Pharm. Sci. 29 (2006) 294–305, https://doi.org/10.1016/J.EJPS.2006.05.013.
[8] S. Mathur, C. Hoskins, Drug development: Lessons from nature, Biomed. Rep. 6 (2017) 612–614, https://doi.org/10.3892/br.2017.909.
[9] C.S. Slater, M.J. Savelski, W.A. Carole, D.J.C. Constable, Solvent Use and Waste Issues, in: Green Chem. Pharm. Ind., John Wiley & Sons, Ltd, 2010, pp. 49–82. 10.1002/9783527629688.CH3.
[10] ICH Official web site. https://www.ich.org/home.html (accessed: February 2022).
[11] F.L. Mota, A.P. Carneiro, A.J. Queimada, S.P. Pinho, E.A. Macedo, Temperature and solvent effects in the solubility of some pharmaceutical compounds: Measurements and modeling, Eur. J. Pharm. Sci. 37 (2009) 499–507, https://doi.org/10.1016/J.EJPS.2009.04.009.
[12] P.A. Patel, P.B. Vandana, AmbiOnp: solid lipid nanoparticles of amphotericin B for oral administration, J. Biomed. Nanotechnol. 7 (2011) 632–639, https://doi.org/10.1166/jbn.2011.1332.
[13] U. Irvin, M. Asher, George Schwartzman, Amphotericin B, Anal. Profiles Drug Subst. Excipients. 6 (1977) 1–42. 10.1016/S0099-5428(08)60338-X.
[14] K.C. Nicolaou, R.A. Daines, T.K. Chakraborty, Y. Ogawa, Total Synthesis of Amphotericin B, J. Am. Chem. Soc. 109 (1987) 2821–2822, https://doi.org/10.1021/ja00243a043.
[15] C. Faustino, L. Pinheiro, Lipid systems for the delivery of amphotericin B in antifungal therapy, Pharmaceutics. 12 (2020) 1–47, https://doi.org/10.3390/pharmaceutics12010029.
[16] M.J. Bryant, S.N. Black, H. Blade, R. Docherty, A.G.P. Maloney, S.C. Taylor, The CSD Drug Subset: The Changing Chemistry and Crystallography of Small Molecule Pharmaceuticals, J. Pharm. Sci. 108 (2019) 1655–1662, https://doi.org/10.1016/J.XPHS.2018.12.011.
[17] K.N. Jarzembska, D. Kamiński, A.A. Hoser, M. Malińska, B. Senczyna, K. Woźniak, M. Gagoś, Controlled Crystallization, Structure, and Molecular Properties of Iodoacetylamphotericin B, Cryst. Growth Des. 12 (2012) 2336–2345, https://doi.org/10.1021/cg2017227.
[18] W.W.H. Zaid Al-Nakeeb, V. Petraitis, J. Goodwin, R. Petraitiene, T.J. Walsh, Pharmacodynamics of amphotericin B deoxycholate, amphotericin B lipid complex, and liposomal amphotericin B against Aspergillus fumigatus, Antimicrob Agents Chemother. 5 (2015) 2735–2745, https://doi.org/10.1128/AAC.04723-14.
[19] L. Mehenni, M. Lahiani-Skiba, G. Ladam, F. Hallouard, M. Skiba, Preparation and Characterization of Spherical Amorphous Solid Dispersion with Amphotericin B, Pharm. 2018, Vol. 10, Page 235. 10 (2018) 235. 10.3390/PHARMACEUTICS10040235.
[20] A. Silva, Study of amphotericin B molecular aggregation into different carrier system, Université Paris Saclay (COmUE); Universidade federal do Rio Grande do Norte (Natal, Brésil), 2017. https://tel.archives-ouvertes.fr/tel-02284561 (accessed August 7, 2021).

[21] C.B. Lim, S.M. Abuzar, P.R. Karn, W. Cho, H.J. Park, C.W. Cho, S.J. Hwang, Preparation, characterization, and in vivo pharmacokinetic study of the supercritical fluid-processed liposomal amphotericin B, Pharmaceutics 11 (2019) 1–18, https://doi.org/10.3390/pharmaceutics11110589.
[22] N. Rajagopalan, M. Dicken, L.J. Ravin, L.A. Sternson, A study of the solubility of amphotericin B in nonaqueous solvent systems, J. Parenter. Sci. Technol. (1988) 97–102. https://www.researchgate.net/publication/19940568 (accessed August 7, 2021).
[23] C. Reichardt, T. Welton, Solvents and Solvent Effects in Organic Chemistry, fourth ed., Wiley-VCH, Weinheim, 2010.
[24] K. Dimroth, C. Reichardt, T. Siepmann, F. Bohlmann, Über Pyridinium-N-phenol-betaine und ihre Verwendung zur Charakterisierung der Polarität von Lösungsmitteln, Justus Liebigs Ann. Chem. 661 (1963) 1–37, https://doi.org/10.1002/jlac.19636610102.
[25] Y. Marcus, The properties of solvents, 1st ed., John Wiley and Sons, New York, 1998.
[26] L. Mehenni, M. Lahiani-Skiba, G. Ladam, F. Hallouard, M. Skiba, Preparation and characterization of spherical amorphous solid dispersion with amphotericin B, Pharmaceutics 10 (2018) 235, https://doi.org/10.3390/pharmaceutics10040235.
[27] M. Charles, Hansen, Hansen Solubility Parameters: A User's Handbook, 2nd ed., CRC Press, Boca Raton, 2007.
[28] R. Soto, M. Svärd, V. Verma, L. Padrela, K. Ryan, Å.C. Rasmuson, Solubility and thermodynamic analysis of ketoprofen in organic solvents, Int. J. Pharm. 588 (2020), https://doi.org/10.1016/j.ijpharm.2020.119686 119686.
[29] H. Buchowski, A. Ksiazczak, S. Pietrzyk, Solvent activity along a saturation line and solubility of hydrogen-bonding solids, J. Phys. Chem. 84 (1980) 975–979, https://doi.org/10.1021/j100446a008.
[30] A. Apelblat, E. Manzurola, Solubilities of L-aspartic, DL-aspartic, DL-glutamic, p-hydroxybenzoic, o-anistic, p-anisic, and itaconic acids in water from T = 278 K to T = 345 K, J. Chem. Thermodyn. 29 (1997) 1527–1533, https://doi.org/10.1006/jcht.1997.0267.
[31] A. Apelblat, E. Manzurola, Solubilities of o-acetylsalicylic, 4-aminosalicylic, 3,5-dinitrosalicylic, and p-toluic acid, and magnesium-DL-aspartate in water from T = (278 to 348) K, J. Chem. Thermodyn. 31 (1999) 85–91, https://doi.org/10.1006/jcht.1998.0424.
[32] R. Soto, V. Verma, M. Sadeghi, Å.C. Rasmuson, Ketoprofen Solubility in Pure Organic Solvents Using In Situ FTIR and UV–Vis and Analysis of Solution Thermodynamics, Org. Process Res. Dev. 25 (2021) 2403–2414, https://doi.org/10.1021/acs.oprd.1c00156.
[33] Y. Zu, W. Sun, X. Zhao, W. Wang, Y. Li, Y. Ge, Y. Liu, K. Wang, Preparation and characterization of amorphous amphotericin B nanoparticles for oral administration through liquid antisolvent precipitation, Eur. J. Pharm. Sci. 53 (2014) 109–117, https://doi.org/10.1016/J.EJPS.2013.12.005.
[34] W.T. Pratthana Chomchalao, Pataranapa Nimtrakul, Duy Toan Pham, Development of amphotericin B-loaded fibroin nanoparticles: a novel approach for topical ocular application, Mater. Life Sci. 55 (2020) 5268–5279. 10.1007/s10853-020-04350-x.
[35] T.T.H. Yen, D.T. Thuan, D.T. Linh, N.V. Khanh, N.T. Hai, P.T.M. Hue, A facile microfluidic method for production of amphotericin B lipid complex, Pharm. Sci. Asia 44 (2017) 200–208. 10.29090/psa.2017.04.200.
[36] C.A. Heffernan, Claire; Soto, Rodrigo; Hodnett. B.Kieran, Rasmuson, C. Heffernan, R. Soto, B.K. Hodnett, A. Rasmuson, Crystal growth kinetics of Curcumin form I, CrystEngComm. in prep (2020). 10.1039/D0CE00034E.
[37] K. Sangwal, Growth kinetics and surface morphology of crystals grown from solutions: Recent observations and their interpretations, Prog. Cryst. Growth Charact. Mater. 36 (1998) 163–248, https://doi.org/10.1016/S0960-8974(98)00009-6.
[38] C.M. Melo, J.F. Cardoso, F.B. Perassoli, A.S. de Oliveira Neto, L.M. Pinto, M.B. de Freitas Marques, W. da Nova Mussel, J.T. Magalhães, S.A. de Lima Moura, M.G. de Freitas Araújo, G.R. Da Silva, Amphotericin B-loaded Eudragit RL100 nanoparticles coated with hyaluronic acid for the treatment of vulvovaginal candidiasis, Carbohydr. Polym. 230 (2020) 115608. 10.1016/J.CARBPOL.2019.115608.
[39] A. Jain, S.H. Yalkowsky, Estimation of melting points of organic compounds-II, J. Pharm. Sci. 95 (2006) 2562–2618, https://doi.org/10.1002/JPS.20634.
[40] C. Salerno, D.A. Chiappetta, A. Arechavala, S. Gorzalczany, S.L. Scioscia, C. Bregni, Lipid-based microtubes for topical delivery of Amphotericin B, Colloids Surfaces B Biointerfaces. 107 (2013) 160–166, https://doi.org/10.1016/J.COLSURFB.2013.02.001.
[41] É.N. Alencar, P. Sawangchan, L.E. Kirsch, E.S.T. Egito, Unveiling the Amphotericin B Degradation Pathway and Its Kinetics in Lipid-Based Solutions, J. Pharm. Sci. 110 (2021) 1248–1258, https://doi.org/10.1016/j.xphs.2020.11.004.
[42] G. Vandermeulen, L. Rouxhet, A. Arien, M.E. Brewster, V. Préat, Encapsulation of amphotericin B in poly(ethylene glycol)-block-poly(ε-caprolactone-co-trimethylenecarbonate) polymeric micelles, Int. J. Pharm. 309 (2006) 234–240, https://doi.org/10.1016/J.IJPHARM.2005.11.031.
[43] K.K. Nishi, M. Antony, P.V. Mohanan, T.V. Anilkumar, P.M. Loiseau, A. Jayakrishnan, Amphotericin B-gum arabic conjugates: synthesis, toxicity, bioavailability, and activities against Leishmania and fungi, Pharm Res. 24 (2007) 971–980, https://doi.org/10.1007/s11095-006-9222-z.
[44] M. Svärd, Å.C. Rasmuson, (Solid+liquid) solubility of organic compounds in organic solvents – Correlation and extrapolation, J. Chem. Thermodyn. 76 (2014) 124–133, https://doi.org/10.1016/j.jct.2014.03.013.
[45] R. Soto, M. Svärd, Solubility and thermodynamic analysis of famotidine polymorphs in pure solvents, Int. J. Pharm. 607 (2021), https://doi.org/10.1016/J.IJPHARM.2021.121031 121031.
[46] F.L. Nordström, Å.C. Rasmuson, Phase Equilibria and Thermodynamics of p-Hydroxybenzoic Acid, J. Pharm. Sci. 95 (2006) 748–760, https://doi.org/10.1002/JPS.20569.